LAWRENCE
LIVERMORE
NATIONAL
LABORATORY

LLNL-JRNL-403004

Plasmon resonance in warm dense matter

R. Thiele, T. Bornath, C. Fortmann, A. Holl, R. Redmer, H. Reinholz, G. Ropke, A. Wierling, S. H. Glenzer, G. Gregori

April 16, 2008

Physics Review Letters

Disclaimer

Plasmon resonance in warm dense matter

R. Thiele,* T. Bornath, C. Fortmann, A. Höll, R. Redmer, H. Reinholz, G. Röpke, and A. Wierling
Institut für Physik, Universität Rostock, D-18051 Rostock, Germany

S.H. Glenzer
L-399, Lawrence Livermore National Laboratory, University of California, P.O. Box 808, Livermore, California 94551, USA

G. Gregori
Clarendon Laboratory, University of Oxford, Parks Road, Oxford, OX1 3PU, CLF, Rutherford Appleton Laboratory, Chilton, Didcot OX11 0QX, United Kingdom

Collective Thomson scattering with extreme ultraviolet light or x-rays is shown to allow for a robust measurement of the free electron density in dense plasmas. Collective excitations like plasmons appear as maxima in the scattering signal. Their frequency position can directly be related to the free electron density. The range of applicability of the standard Gross-Bohm dispersion relation and of an improved dispersion relation in comparison to calculations based on the dielectric function in random phase approximation is investigated. More important, this well-established treatment of Thomson scattering on free electrons is generalized in the Born-Mermin approximation by including collisions. We show that, in the transition region from collective to non-collective scattering, the consideration of collisions is important.

PACS numbers: 52.25.Os, 52.35.Fp, 71.45.Gm, 71.10.Ca
Keywords: Warm dense matter; Plasma diagnostics; Thomson scattering; Plasmons

I. INTRODUCTION

A key issue in the diagnostics of dense plasmas is the determination of the free electron density and temperature. Physical properties such as line profiles, bremsstrahlung spectrum or Thomson scattering can be used for that purpose. In this context, the knowledge of the plasmon resonance is necessary for the analysis of experimental data. Therefore, we discuss the applicability of the Gross-Bohm dispersion relation and options to go beyond it when considering the determination of plasma parameters in warm dense matter (WDM), where many-particle effects like collisions play an important role.

The region of WDM considered is relevant for, e.g., inertial confinement fusion experiments or models for planetary interiors. WDM is characterized by a free electron density of $n_e = 10^{22} - 10^{26}\,\mathrm{cm}^{-3}$ and temperatures of several eV. These plasmas are opaque in the optical region since the frequency of light $\omega_0 = 2\pi c/\lambda_0$ is lower than the plasma frequency $\omega_{\mathrm{pe}}^2 = n_e e^2/(\epsilon_0 m_e)$ of the free electron subsystem, with the electron density n_e and the electron mass m_e. Therefore, probing plasmas with densities approaching solids or even higher densities requires x-ray sources.

Powerful x-ray pulses are produced by energetic optical lasers [1] and then used to pump and probe samples in the near-solid density regime. The 4.75 keV titanium He-α backlighter [2, 3] has been used to perform non-collective Thomson scattering spectrum on solid density beryllium. From the shape of the Compton shifted electron scattering signal, the electron temperature could be detected. In a another pioneering experiment, scattering from the collective electron plasma mode (plasmon) at solid density beryllium using a Cl Ly-α backlighter at 2.96 keV was also performed [4].

Alternatively, the study of WDM will eventually be possible with new 4th generation light sources (FEL-free electron lasers in the VUV and x-ray region) as a tool to probe near-solid density targets. Currently available is the FLASH facility at DESY, Hamburg, with wavelengths ranging from $7 - 50\,\mathrm{nm}$ in the VUV region [5, 6]. The construction of an x-ray FEL is planned at DESY [7, 8] in 2013. A similar project is currently under construction at the Stanford Linear Acceleration Center (SLAC) [9].

In plasmas at near solid density, strong coupling effects are important. In particular, a consistent many-body theory is needed if the nonideality parameter Γ_e for electrons

$$\Gamma_e = \frac{e^2}{4\pi\epsilon_0 k_{\mathrm{B}} T_e}\left(\frac{4\pi n_e}{3}\right)^{1/3} \tag{1}$$

is larger than 1. The plasma parameters, i.e. the free electron temperature T_e and the free electron density n_e, as well as the ionization state Z, can be derived analyzing the Thomson scattering signal. The electron temperature can be obtained using the method of detailed balance [4, 10], while the electron density follows from the plasmon dispersion relation for collective scattering. In this paper, we discuss the measurement of the free electron density via the maximum position of the plas-

*Electronic address: robert.thiele@uni-rostock.de

mon peak. We compare with the usual Gross-Bohm [11] dispersion relation $\omega_{\rm GB}(k)$. Furthermore, we analyze the improved dispersion relation (IDR) [10] accounting for higher density effects, characterized by the degeneracy parameter Θ_e for electrons

$$\Theta_e = \frac{2m_e k_{\rm B} T_e}{\hbar^2}(3\pi^2 n_e)^{-2/3} \ , \tag{2}$$

and higher orders of the scattering wavenumber. In Ref. [12], analytic results for the dynamic structure factor as the basic input for the Thomson scattering cross section on the level of the random phase approximation (RPA) were shown. Recently, the influence of collisions on the dynamic structure factor [13] was studied. A systematic improvement of the Born approximation including dynamic screening and strong collisions [14, 15] has been accomplished by use of thermodynamic Green's functions leading to the Gould-DeWitt [16] scheme. This can be extended to finite wavenumbers k by the Mermin approach [17–19] in order to calculate the dynamic structure factor.

For the interpretation and evaluation of state-of-the-art plasma experiments, accurate measurements of the Thomson scattering signal are needed. Therefore, the scattering of photons on plasmas has been studied for a long time [20–24]. We will show that Thomson scattering can indeed serve as a reliable diagnostic tool to analyze plasma parameters as, e.g., density, temperature, and plasma composition or to test the quality of the models used to determine the dynamic structure factor.

In the next section, we introduce the dynamic structure factor and the Born-Mermin approximation (BMA). In Section III, we study the position of the plasmon peak under the influence of collisions. The Gross-Bohm plasmon dispersion relation and the IDR are described in Section IV. The results for solid density plasmas are shown in Section V. We will conclude with a summary.

II. DYNAMIC STRUCTURE FACTOR

As described in [12, 21, 24, 25], the experimental Thomson scattering cross section is related to the dynamic structure factor of all electrons in the plasma according to

$$\frac{d^2\sigma}{d\Omega d\omega} = \sigma_T \frac{k_1}{k_0} S_{ee}(k,\omega) \ . \tag{3}$$

Here, $\sigma_T = 6.65\times10^{-29}\,\mathrm{m}^2$ is the Thomson cross section, k_0 and k_1 are the wavenumbers of the incident and the scattered light, the energy and momentum transfer are given by $\Delta E = \hbar\omega = \hbar\omega_1 - \hbar\omega_0$ and $\hbar\mathbf{k} = \hbar\mathbf{k}_1 - \hbar\mathbf{k}_0$. The momentum is related to the scattering angle θ in the limit $\hbar\omega \ll \hbar\omega_0$ according to $k = 4\pi\sin(\theta/2)/\lambda_0$. Here, we follow Chihara's approach [21, 24], in that the

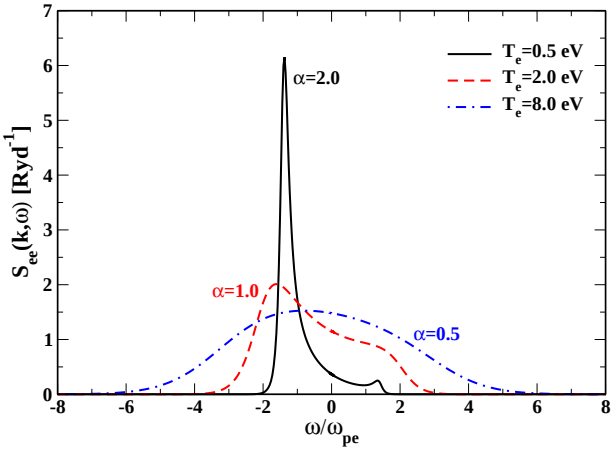

FIG. 1: (color online) Electronic dynamic structure factor $S_{ee}(k,\omega)$ from collective ($\alpha = 2.0$) up to non-collective ($\alpha = 0.5$) Thomson scattering calculated in BMA for a fully ionized hydrogen plasma with $n_e = 10^{21}\,\mathrm{cm}^{-3}$, a laser wavelength $\lambda_0 = 4.13\,\mathrm{nm}$, and a scattering angle $\theta_S = 160°$.

total dynamic structure factor can be written in terms of contributions from free electrons, weakly and tightly bound electrons, and core electrons. In this paper, the dynamic structure factor of free electrons is considered.

In thermodynamic equilibrium, the dynamic structure factor $S_{ee}(k,\omega)$ and the longitudinal dielectric function $\epsilon(k,\omega)$ are related via the fluctuation-dissipation theorem

$$S_{ee}(k,\omega) = -\frac{\epsilon_0\hbar k^2}{\pi e^2 n_e}\frac{\mathrm{Im}\,\epsilon^{-1}(k,\omega)}{1-\exp\left(-\frac{\hbar\omega}{k_B T_e}\right)} \ . \tag{4}$$

A peak in the dynamic structure factor or in the imaginary part of the inverse dielectric function,

$$\mathrm{Im}\,\epsilon^{-1}(k,\omega) = \frac{-\mathrm{Im}\,\epsilon(k,\omega)}{[\mathrm{Re}\,\epsilon(k,\omega)]^2 + [\mathrm{Im}\,\epsilon(k,\omega)]^2} \ , \tag{5}$$

can be interpreted as a resonant charge density excitation or plasmon. In general, the dielectric function is given in terms of the polarization function $\Pi(\vec{k},\omega)$ via

$$\epsilon(\vec{k},\omega) = 1 - \frac{1}{\epsilon_0 k^2}\Pi(\vec{k},\omega) \ . \tag{6}$$

Neglecting collisions, the polarization function is given in RPA as

$$\Pi^{\rm RPA}(\mathbf{k},\omega) = \frac{1}{\Omega_0}\sum_p e^2 \frac{f^e_{p+k/2} - f^e_{p-k/2}}{\Delta E^e_{p,k} - \hbar(\omega + \mathrm{i}\eta)} \ . \tag{7}$$

Here, Ω_0 is the normalization volume and $\Delta E^e_{p,k} = E^e_{p+k/2} - E^e_{p-k/2} = \hbar^2\mathbf{k}\cdot\mathbf{p}/m_e$. Furthermore, $f^e_p = [\exp(E^e_p - \mu_e)/k_B T_e + 1]^{-1}$ denotes the Fermi distribution function, μ_e the chemical potential of the electrons. The

limit $\eta \to 0$ has to be taken after the thermodynamic limit.

We improve the RPA by considering collisions if using a Drude-like behavior for the damping of the frequency dependent dielectric function via a collision frequency. Within linear response theory [19], the dynamic collision frequency $\nu(\omega)$ can be consistently introduced via the Mermin dielectric function

$$\epsilon^{\rm M}(k,\omega) - 1 = \frac{\left(1 + {\rm i}\frac{\nu(\omega)}{\omega}\right)\left[\epsilon^{\rm RPA}(k,\omega + {\rm i}\nu(\omega)) - 1\right]}{1 + {\rm i}\frac{\nu(\omega)}{\omega}\frac{\epsilon^{\rm RPA}(k,\omega+{\rm i}\nu(\omega))-1}{\epsilon^{\rm RPA}(k,0)-1}} . \quad (8)$$

In [13, 25], the influence of collisions on the dynamic structure factor was investigated for a wide range of temperatures and densities applying various approximations. In this paper, we will evaluate the collision frequency in Born approximation with respect to a statically screened Debye potential which can be written [10, 14, 15] as

$$\begin{aligned}\nu^{\rm Born}(\omega) &= -{\rm i}\frac{\epsilon_0 n_i \Omega_0^2}{6\pi^2 e^2 n_e m_e}\frac{1}{\omega}\int_0^\infty dq\, q^6 V_D^2(q) S_{ii}(q) \\ &\quad \times \left[\epsilon^{\rm RPA}(q,\omega) - \epsilon^{\rm RPA}(q,0)\right] , \end{aligned} \quad (9)$$

with $S_{ii}(q)$ being the static ion-ion structure factor and $V_D(q) = -Ze^2/(\epsilon_0\Omega_0(q^2+\kappa^2))$ the statically screened electron-ion Debye potential. κ is the inverse screening length in the plasma which is given for plasmas at any degeneracy by

$$\kappa^2 = \frac{e^2 m_e^{3/2}}{\sqrt{2}\pi^2\epsilon_0\hbar^3}\int_0^\infty dE_p\, E_p^{-1/2} f_p^e . \quad (10)$$

In the classical case, the well-known inverse Debye screening $\kappa_D^2 = n_e e^2/(\epsilon_0 k_B T_e)$ is obtained.

Applying to scattering experiment in warm dense matter, the range of the wavenumber k is of interest, which is given by the experimental setup. It allows to discriminate collective and non-collective scattering. Therefore, to further analyze the structure factor and Thomson scattering, the scattering parameter [26]

$$\alpha = \frac{\kappa}{k} \quad (11)$$

is introduced. For $\alpha < 1$, the scattering is non-collective, and we can investigate short-range correlations within the Debye sphere [1]. Long-range correlations are relevant for collective scattering ($\alpha > 1$). In this case, the electronic structure factor $S_{ee}(k,\omega)$, shows two particularly pronounced side maxima found symmetrically to the central Rayleigh peak which are related to the free electron density, see also [4]. In the following we will restrict ourselves to the red shifted peak since it is the one with the higher intensity.

In Fig. 1, the electronic dynamic structure factor $S_{ee}(k,\omega)$ in BMA is shown for different conditions. For collective scattering ($\alpha = 2.0$), we see a sharp peak near the electronic plasma frequency $\omega_{\rm pe}$. For non-collective scattering ($\alpha = 0.5$), only one maximum of $S_{ee}(k,\omega)$ is found and the peak is broadened due to thermal electronic motion. Within our approach, we now consider collective scattering with a scattering parameter $\alpha > 1$. We will present results for the dielectric function in Born-Mermin approximation, where the maximum position $S_{ee}^{\rm max}(k,\omega)$ is determined numerically as a function of density and temperature. Nevertheless, it is useful for plasma diagnostics to have analytical estimates for the peak position. We will aim at an improved plasmon dispersion relation below.

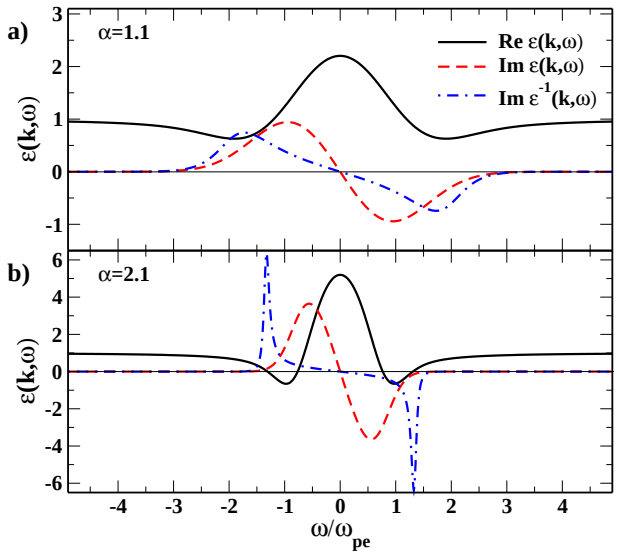

FIG. 2: (color online) Dielectric function $\epsilon^{\rm RPA}(k,\omega)$ of electrons for electron densities: a) $n_e = 1.0\times10^{23}\,{\rm cm}^{-3}$ ($\alpha = 1.1$) and b) $n_e = 5.0\times10^{23}\,{\rm cm}^{-3}$ ($\alpha = 2.1$). The electron temperature is $T_e = 12\,{\rm eV}$, laser wavelength $\lambda_0 = 0.42\,{\rm nm}$, and the scattering angle $\theta_S = 40°$.

III. POSITION OF PLASMON PEAK IN THE DRUDE LIMIT

In the following, we will discuss the position of the maximum in the dynamic structure factor $S_{ee}(k,\omega)$ which is due to a red shift of the probing frequency and is related to the imaginary part of the inverse dielectric function according to Eq. (4). In the collective regime, the maximum position is the so-called plasmon peak or plasmon resonance. For strong collective scattering ($\alpha \gg 1$), it is the long-wavelength limit ($k \to 0$).

In Fig. 2, the real and imaginary parts of the dielectric function, and the imaginary part of the inverse dielectric function, all calculated within RPA, Eq. (6) using Eq. (7), are shown for weakly collective ($\alpha = 1.1$) and collective ($\alpha = 2.1$) scattering. For $\alpha = 2.1$, the real part of the dielectric function has four zeros. The plasmon peak of interest can be found at the zero of ${\rm Re}\,\epsilon(k,\omega)$ with the

highest absolute value of the frequency shift, because the imaginary part is minimal. Here, a narrow sharp peak of $\mathrm{Im}\,\epsilon^{-1}(k,\omega)$ can be found, typical for collective scattering. In the other case, for $\alpha = 1.1$, a zero of the real part of the dielectric function does not exist.

For an estimate of the influence of collisions, we discuss the position of the plasmon peak within the Drude model [27, 28], obtained from the Mermin formula Eq. (8) in the long-wavelength limit

$$\lim_{k\to 0} \epsilon^{\mathrm{M}}(k,\omega) = \epsilon(\omega) = 1 - \frac{\omega_{\mathrm{pe}}^2}{\omega[\omega + \mathrm{i}\nu(\omega)]} \ . \tag{12}$$

In the case of a static collision frequency $\nu = \nu(0)$, and $\mathrm{Im}\,\nu = 0$, the real and the imaginary part of the dielectric function are given by

$$\mathrm{Re}\,\epsilon(\omega) = \frac{\omega^2 + \nu^2 - \omega_{\mathrm{pe}}^2}{\omega^2 + \nu^2} \ , \ \mathrm{Im}\,\epsilon(\omega) = \frac{\nu}{\omega}\frac{\omega_{\mathrm{pe}}^2}{\omega^2 + \nu^2} \ . \tag{13}$$

As a result, the imaginary part of the inverse dielectric function can be written in the following form

$$\mathrm{Im}\,\epsilon^{-1}(\omega) = \frac{\nu\omega\omega_{\mathrm{pe}}^2(\omega^2 + \nu^2)}{\omega^2(\omega^2 + \nu^2 - \omega_{\mathrm{pe}}^2)^2 + \nu^2\omega_{\mathrm{pe}}^4} \ . \tag{14}$$

The maximum position of $S_{ee}(k,\omega)$ can be found at

$$\omega_{\mathrm{res}}^2 \approx \omega_{\mathrm{pe}}^2 - \frac{\nu^2}{4} \ , \tag{15}$$

assuming $\nu \ll \omega_{\mathrm{pe}}$. Thus, the plasmon peak is expected to shift due to collisions. In [25], the static collision frequency, normalized by the electronic plasma frequency, was shown for a wide range of free electron densities. It was found, that $\nu \approx \omega_{\mathrm{pe}}$ only in the density region of $n_e = 10^{21}\,\mathrm{cm}^{-3}$ if typical temperatures for WDM are considered. Otherwise $\nu \ll \omega_{\mathrm{pe}}$ [13] applies.

In contrast to Eq. (15), an estimate of the maximum position of $S_{ee}(k,\omega)$ from the dispersion relation $\mathrm{Re}\,\epsilon(\omega) = 0$, Eq. (13) leads to

$$\omega_0^2 = \omega_{\mathrm{pe}}^2 - \nu^2 = \omega_{\mathrm{pe}}^2\left(1 - \frac{\nu^2}{\omega_{\mathrm{pe}}^2}\right) \ . \tag{16}$$

In conclusion, for both expressions, the shift of the plasmon peak is a function of ν/ω_{pe}. Thus, for $\nu \ll \omega_{\mathrm{pe}}$, the effect of collisions on the position of the plasmon peak can be neglected, as we will see later in numerical results. Therefore, we will derive the plasmon dispersion relation in RPA.

IV. PLASMON DISPERSION RELATION

Generally spoken, plasmons can be found as poles of $1/\epsilon(k,z)$ in the lower complex half plane ($\mathrm{Im}\,z < 0$) [29]. There are no analytical results available, however. Assuming small $\mathrm{Im}\,\epsilon(k,\omega)$, the peak is essentially determined by the solution of the dispersion relation

$$\mathrm{Re}\,\epsilon(k,\omega)|_{\omega=\omega_0(k)} = 0 \tag{17}$$

or, at least, by a minimum of $\mathrm{Re}\,\epsilon(k,\omega)$. Considering the case of the RPA, we present plasmon dispersion relations in different approximations.

Starting from the Lindhard formula, see Eq. (7), the real part of the dielectric function can be written as [30]

$$\begin{aligned}\mathrm{Re}\,\epsilon(k,\omega) &= 1 - \frac{\omega_{\mathrm{pe}}^2}{\omega^2} \\ &\times \left[1 + \frac{z^2}{u^2} + \frac{3}{2}\frac{F_{3/2}(\eta)}{u^2 D^{5/2}} + \frac{3}{2}\frac{F_{5/2}(\eta)}{u^4 D^{7/2}} + \ldots\right]\end{aligned} \tag{18}$$

for $z \ll u$, with $u = \omega/kv_F$, $z = k/2k_F$, $\eta = \mu_e/k_BT_e$ and $D = 1/\Theta_e$. The velocity v_F corresponds to the Fermi wavenumber $k_F = m_e v_F/\hbar = (3\pi^2 n_e)^{1/3}$. The Fermi integrals $F_j(x)$ are defined by Eq. (A.3). From $z \ll u$, the condition $k \ll \sqrt{2m_e\omega/\hbar}$ is derived. This limits the applicability of Eq. (18) to scattering parameters

$$\alpha \gg \sqrt{\frac{\hbar\omega_{\mathrm{pe}}}{2k_BT_e}} \ . \tag{19}$$

Assuming approximation Eq. (18), the dispersion relation Eq. (17) for the RPA is solved by

$$\begin{aligned}\omega_0^2(k) &= \omega_{\mathrm{pe}}^2 \\ &\times \left[1 + \frac{\langle p^2\rangle}{m_e^2}\frac{k^2}{\omega_0^2} + \frac{\langle p^4\rangle}{m_e^4}\frac{k^4}{\omega_0^4} + \left(\frac{\hbar}{2m_e}\right)^2\frac{k^4}{\omega_0^2} + \ldots\right]\end{aligned} \tag{20}$$

with the moments $\langle p^i\rangle$ related to the Fermi intergrals and defined by Eq. (A.1).

In the classical limit, $\lim_{\Theta\gg 1}\langle p^2\rangle = 3k_BT_em_e$, and by neglecting terms beyond the order of k^2, we obtain the well-known Gross-Bohm dispersion relation [11]

$$\omega_{\mathrm{GB}}^2(k) = \omega_{\mathrm{pe}}^2 + \frac{3k_BT_e}{m_e}k^2 \ . \tag{21}$$

The plasmon resonance in the Gross-Bohm relation ω_{GB} is approximated by the electron plasma frequency ω_{pe} and an additional term which depends on electron temperature and scattering wavenumber only.

For a weakly degenerate electron gas with $\Theta \approx 1$, the Fermi intergrals can be expanded, see Eq. (A.4).Taking this into account as well as the next order of k, we derive the improved dispersion relation (IDR)

$$\omega_{\mathrm{IDR}}^2 = \omega_{\mathrm{pe}}^2 + \frac{3k_BT_e}{m_e}k^2(1 + 0.088n_e\Lambda_e^3) + \left(\frac{\hbar k^2}{2m_e}\right)^2 \ . \tag{22}$$

In comparison to the Gross-Bohm dispersion relation, the range of applicability is extended to higher wavenumbers (larger scattering angles) and higher densities (or lower temperatures).

V. RESULTS FOR WDM

We will now compare the position of the maximum of the dynamic structure factor $S_{ee}(k,\omega)$ in RPA, see Eq. (4) - Eq. (7) and BMA, see Eq. (4) - Eq. (9) with the resonance frequency $\omega_{\rm IDR}$, Eq. (22).

First, we calculate these quantities for a fully ionized hydrogen plasma in the electron density range $n_e = (10^{20}\ldots10^{22})\,\mathrm{cm}^{-3}$, the laser wavelength $\lambda_0 = 25\,\mathrm{nm}$, and scattering angle $\theta_S = 90°$. These conditions are relevant for collective Thomson scattering experiments at FLASH [10]. In Fig. 3, the position of the maximum of $S_{ee}(k,\omega)$ as a function of the density of free electrons for the RPA and the BMA for different temperatures ($T_e = 0.5, 3, 15\,\mathrm{eV}$) is shown. Furthermore, we compare the calculations with the energy shift $\omega_{\rm IDR}$. In the density range investigated here, the differences between Gross-Bohm and IDR are very small, so that only the IDR results are shown. For all temperatures in the range of $T_e = (0.5\ldots15)\,\mathrm{eV}$, the differences between the RPA, the BMA, and the IDR are less than 5%. The resonance frequency $\omega_{\rm IDR}$ shows the square root dependence on the electron density.

In the insets, the maximum position of $S_{ee}(k,\omega)$ is shown for the lower density range starting at $7.5\times10^{19}\,\mathrm{cm}^{-3}$ of the free electron density. The frequency shift is related to the electron plasma frequency. Towards lower densities and higher temperatures, where a transition from collective to non-collective scattering occurs, stronger deviations of the dispersion relations from the numerical results are observed, in particular for the 15 eV curves in Fig. 3. For $T_e = 15\,\mathrm{eV}$, the scattering parameter is $\alpha = 0.85$ at $n_e = 7.5\times10^{19}\,\mathrm{cm}^{-3}$, and $\alpha > 10$ at the highest density $n_e = 1.0\times10^{22}\,\mathrm{cm}^{-3}$. The Gross-Bohm relation and IDR are approximations for zeros of the real part of the dielectric function, $\mathrm{Re}\,\epsilon(k,\omega) = 0$. In the non-collective scattering region, however, the zeros do not exist. Therefore, the Gross-Bohm dispersion relation and also the IDR are not applicable for the transition region and for non-collective scattering parameters. Nevertheless, the maximum in the structure factor as calculated by BMA or RPA can be used to infer the density from experimental plasmon spectra. However, the maximum is less pronounced and experimentally less well detectable.

In a next example, a beryllium plasma is produced and investigated in pump-probe experiments at the Omega laser facility [4, 32] with wavelength $\lambda_0 = 0.42\,\mathrm{nm}$. Electron temperatures of $T_e = 12\,\mathrm{eV}$ are obtained and the scattering signal is observed at an angle $\theta_S = 40°$. In Fig. 4, the dependence of the maximum position of $S_{ee}(k,\omega)$ in RPA and BMA on the free electron density are shown, together with the energy shift in IDR and Gross-Bohm, and the zeros of the real part of the dielectric function in RPA. Additionally, we compare with results following from the dielectric function which was calculated including local field corrections (LFC) [31] and an experimental point taken from [4]. In the considered density range, the differences between the structure fac-

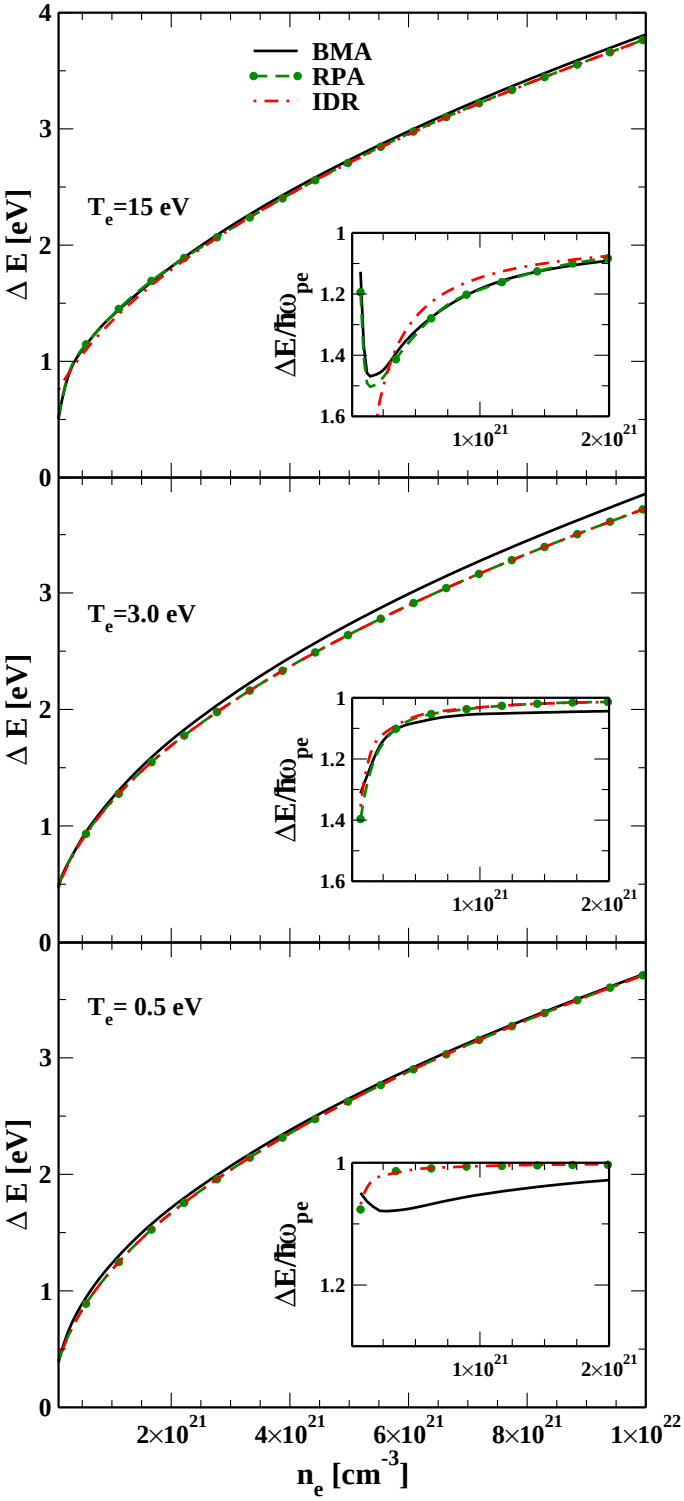

FIG. 3: (color online) Comparison of the maximum position ΔE of $S_{ee}(k,\omega)$ in RPA (green-dotted line) and BMA (black-solid line) with the energy shift $\omega_{\rm IDR}$ (red-dashed-dotted line) in dependence on electron density n_e for a fully-ionized hydrogen plasma with the laser wavelength $\lambda_0 = 25\,\mathrm{nm}$ and scattering angle $\theta_S = 90°$. The insets show the normalized energy shift for the lower densities.

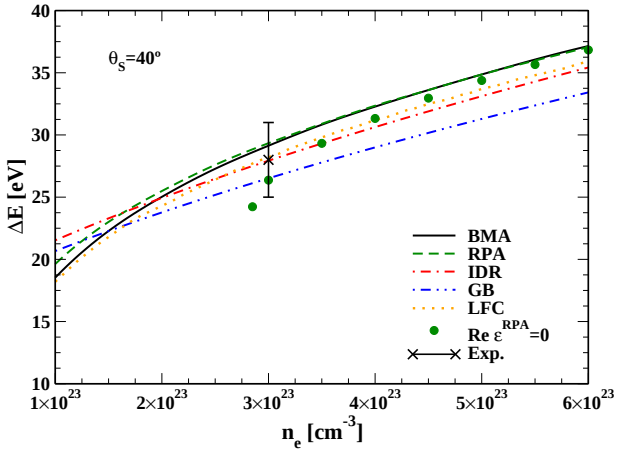

FIG. 4: (color online) Comparison of the maximum position ΔE of $S_{ee}(k,\omega)$ in RPA (green-dashed line) and BMA (black-solid line) with the energy shift in GB dispersion relation (blue-dashed-dot-dotted line) and IDR (red-dashed-dotted line) and local field corrections (LFC: orange-dotted line) [31] in dependence on electron density n_e for a beryllium plasma with $Z_{\rm eff} = 2.5$, $T_e = 12\,\mathrm{eV}$, and the laser wavelength $\lambda_0 = 0.42\,\mathrm{nm}$ and scattering angle $\theta_S = 40°$. The green points are the zeros of $\mathrm{Re}\,\epsilon(k,\omega)$ and the experimental point is taken from [4].

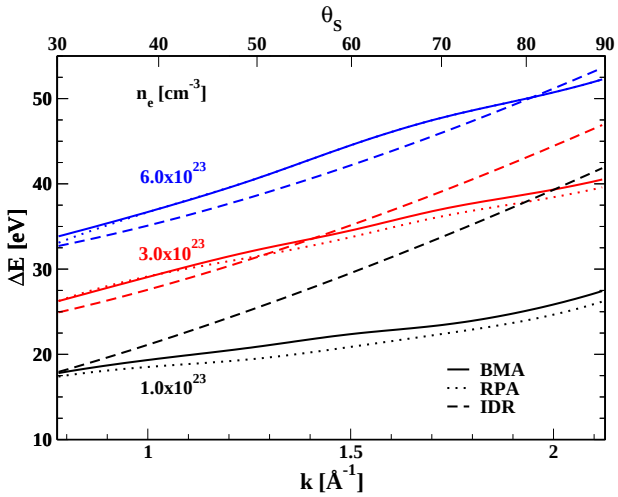

FIG. 5: (color online) Comparison of the maximum position ΔE of $S_{ee}(k,\omega)$ in RPA (dotted line) and in BMA (solid line) with the energy shift of the IDR (dashed line) in dependence on wavenumber k and scattering angle θ_S respectively for Thomson scattering on beryllium plasma with $Z_{\rm eff} = 2.5$, $n_e = 1, 3, 6 \times 10^{23}\,\mathrm{cm}^{-3}$, $T_e = 12\,\mathrm{eV}$, and the laser wavelength $\lambda_0 = 0.42\,\mathrm{nm}$.

tor calculations and the dispersion relations are considerable. For densities smaller than $n_e = 2.8 \times 10^{23}\,\mathrm{cm}^{-3}$, the scattering parameter α is lower than one, and zeros of $\mathrm{Re}\,\epsilon(k,\omega)$ do not exist. Again, GB and IDR are not applicable. The shift of the maximum position obtained from the BMA is smaller compared to the RPA due to the relevance of collisions in this region.

For higher densities ($n_e \geq 4.0 \times 10^{23}\,\mathrm{cm}^{-3}$), the maximum position is not affected by collisions. BMA and RPA give the same result. For strongly collective regime, the zeros of the real part of the dielectric function can be found at the same energy as the maximum position of $S_{ee}(k,\omega)$. However note, for high densities and collective scattering, the difference between the Gross-Bohm dispersion relation and BMA is $\Delta E \approx 4\,\mathrm{eV}$. The improved dispersion relation with respect to quantum effects underestimates the energy shift with $\Delta E \approx 2\,\mathrm{eV}$. These differences are significant, a few eV shift make an error of more than 30% in the free electron density.

Fig. 5 shows the energy shift of the Thomson scattering signal for different free electron densities in dependence on wavenumber k and scattering angle θ_S. The scattering parameter α decreases with increasing wavenumber or scattering angle, and decreasing electron density. For $n_e = 1.0 \times 10^{23}\,\mathrm{cm}^{-3}$, the scattering angle varies from $\alpha = 1.5$ to $\alpha = 0.5$ for $\theta_S = 30^o$ to $\theta_S = 90^o$, respectively. For $\theta > 40^o$, the scattering is non-collective. Therefore, the difference between IDR and BMA is significant for higher wavenumbers and towards lower densities, whereas collisions can be neglected. However, in the region of non-collective scattering the BMA is superior to the RPA.

VI. SUMMARY

We have discussed the plasmon resonance position of the dynamic structure factor $S_{ee}(k,\omega)$, the usual Gross-Bohm dispersion relation, and the improved dispersion relation. This is relevant for the determination of the free electron density in warm dense matter. Firstly, we calculated the energy shift observed for a fully ionized hydrogen plasma. Here, the differences between the dispersion relations and the maximum position of the dynamic structure factor in RPA and BMA are small. Only for the determination of the free electron density in the transition region between non-collective and collective scattering, the BMA is needed. For solid targets probed by x-ray wavelength, the density should be calculated from the maximum position of $S_{ee}(k,\omega)$ in BMA. In this region, the usual dispersion relations (GB and IDR) are not justified.

In this paper, we have shown a method to derive the free electron density via the resonance position of the electronic dynamic structure factor in BMA in comparison with the estimated resonance position via the usual dispersion relations. We demonstrate that the dispersion relations are not suited for the density determination in the solid-density region. Collision effects are very important [13] and can be considered within the BMA. A reliable density determination can only be done by numerically solving the BMA and inspecting the poles of $\mathrm{Im}\,\epsilon^{-1}(k,\omega)$.

Acknowledgments

This work was supported by the virtual institute VH-VI-104 of the Helmholtz association and the Sonderforschungsbereich SFB 652. The work by SHG was performed under the auspices of the U.S. Department of Energy by Lawrence Livermore National Laboratory under Contract DE-AC52-07NA27344. SHG was also supported by LDRDs 08-ERI-002, 08-LW-004, and the Alexander-von-Humboldt foundation. The work of GG was partially supported by the Science and Technology Facilities Council of the United Kingdom.

APPENDIX

We discuss the calculation of Eq. (20). The prefactors $\langle p^i \rangle$ are defined as [30]

$$\langle p^i \rangle = \frac{g_s}{n_e} \int \frac{\mathrm{d}^3 p}{(2\pi)^3} p^i \, f_e(p) \,. \tag{A.1}$$

The prefactor $\langle p^2 \rangle$ of the k^2-term in Eq. (20) is proportional to the mean energy of the (ideal) Fermi system and allows, therefore, to incorporate quantum statistical corrections. Especially, we have

$$\langle p^2 \rangle = \frac{3}{2} k_B T \, \frac{1}{y} F_{3/2}(x) \,, \tag{A.2}$$

with the parameter $y = n_e \Lambda_e^3 / g_s$, the thermal wave length $\Lambda_e = h/\sqrt{2\pi m_e k_B T}$, $x = \beta\mu$, and the Fermi integrals

$$F_j(x) = \frac{1}{\Gamma(j+1)} \int_0^\infty \frac{t^j \mathrm{d}t}{\mathrm{e}^{t-x}+1} \,. \tag{A.3}$$

In order to supply the reader with tractable expressions [33, 34], we give the following result

$$F_{3/2}(y) \tag{A.4}$$
$$= \begin{cases} y + 0.1768\, y^2 - 0.0033\, y^3 + 0.000094\, y^4 \,, & y < 5.5 \\ 0.4836\, y^{5/3} + 1.3606\, y^{1/3} - 1.7\, y^{-1} \,, & y > 5.5 \,. \end{cases}$$

The parameter y can be estimated from $y = 0.1656 (n_e/10^{21}\mathrm{cm}^{-3})/(k_B T/\mathrm{eV})^{3/2}$. For $y \leq 2$, one can use $1/y\, F_{3/2}(y) = 1 + 0.1768\, y$ making an error less than 1%. With Eq. (A.4), the equation Eq. (20) can be solved to the order of k^4, and we get Eq. (22).

[1] O. L. Landen, S. H. Glenzer, M. J. Edwards, R. W. Lee, G. W. Collins, R. C. Cauble, W. W. Hsing, and B. A. Hammel, J. Quant. Spectrosc. Radiat. Transfer **71**, 465 (2001).
[2] S. H. Glenzer, G. Gregori, R. W. Lee, F. J. Rogers, S. W. Pollaine, and O. L. Landen, Phys. Rev. Lett. **90**, 175002 (2003).
[3] S. H. Glenzer, G. Gregori, F. J. Rogers, D. H. Froula, S. W. Pollaine, R. S. Wallace, and O. L. Landen, Phys. Plasmas **10**, 2433 (2003).
[4] S. H. Glenzer, O. L. Landen, P. Neumayer, R. W. Lee, K. Widmann, S. W. Pollaine, R. J. Wallace, G. Gregori, A. Höll, T. Bornath, et al., Phys. Rev. Lett. **98**, 065002 (2007).
[5] A. Kondratenko and E. Saldin, Part. Acc. **10**, 207 (1980).
[6] R. Bonifacio, C. Pellegrini, and L. Narducci, Opt. Comm. **50**, 373 (1984).
[7] G. Materlik and T. Tschentscher, eds., *TESLA - Technical Design Report Part V: The X-Ray Free Electron Laser* (DESY Report 2001-011, Hamburg, 2001).
[8] R. Brinkmann, K. F. B. Faatz, J. Rossbach, J. R. Schneider, H. Schulte-Schrepping, D. Trines, T. Tschentscher, and H. Weise, eds., *TESLA XFEL Technical Design Report (Supplement)* (DESY, Hamburg, Germany, DESY Rep. 2002-167, 2002).
[9] *LCLS Design Study Report* (The LCLS Design Study Group, SLAC, Stanford, CA, 1998), SLAC-R-0521.
[10] A. Höll, T. Bornath, L. Cao, T. Döppner, S. Düsterer, E. Förster, C. Fortmann, S. H. Glenzer, G. Gregori, T. Laarmann, et al., High Energy Dens. Phys. **3**, 120 (2007).
[11] D. Bohm and E. P. Gross, Phys. Rev. **75**, 1851 (1949).
[12] G. Gregori, S. H. Glenzer, W. Rozmus, R. W. Lee, and O. L. Landen, Phys. Rev. E **67**, 026412 (2003).
[13] A. Höll, R. Redmer, G. Röpke, and H. Reinholz, Eur. Phys. J. D **29**, 159 (2004).
[14] H. Reinholz, R. Redmer, G. Röpke, and A. Wierling, Phys. Rev. E **62**, 5648 (2000).
[15] R. Thiele, R. Redmer, H. Reinholz, and G. Röpke, J. Phys. A **39**, 4365 (2006).
[16] H. A. Gould and H. E. DeWitt, Phys. Rev. **155**, 68 (1967).
[17] N. D. Mermin, Phys. Rev. B **1**, 2362 (1970).
[18] A. W. G. Röpke, A. Selchow and H. Reinholz, Phys. Lett. A **260**, 365 (1999).
[19] A. Selchow, G. Röpke, A. Wierling, H. Reinholz, T. Pschiwul, and G. Zwicknagel, Phys. Rev. E **64**, 056410 (2001).
[20] D. E. Evans and J. Katzenstein, Rep. Progr. Phys. **32**, 207 (1969).
[21] J. Chihara, J. Phys. F **17**, 295 (1987).
[22] V. N. Tsytovich, Astropart. Phys. **5**, 285 (1996).
[23] E. Nardi, Z. Zinamon, D. Riley, and N. C. Woolsey, Phys. Rev. E **57**, 4693 (1998).
[24] J. Chihara, J. Phys. Cond. Matter **12**, 231 (2000).
[25] R. Redmer, H. Reinholz, G. Röpke, R. Thiele, and A. Höll, IEEE Trans. on Plasma Sci. **33**, 77 (2005).
[26] E. E. Salpeter, Phys. Rev. **120**, 1528 (1960).
[27] P. Drude, Ann. Phys. (Leipzig) **39**, 504 (1890).
[28] A. Selchow, G. Röpke, and A. Wierling, Contrib. Plasma Phys. **42**, 43 (2002).
[29] W. Kraeft, D. Kremp, W. Ebeling, and G. Röpke, *Quan-*

tum Statistics of Charged Particle Systems (Akademie-Verlag, Berlin, 1986).
[30] N. R. Arista and W. Brandt, Phys. Rev. A **29**, 1471 (1984).
[31] G. Gregori, A. Ravasio, A. Höll, S. Glenzer, and S. Rose, High Energy Dens. Phys. **3**, 99 (2007).
[32] J. M. Soures, R. L. McCrory, C. P. Verdon, A. Babushkin, R. E. Bahr, T. R. Boehly, R. Boni, D. K. Bradley, D. L. Brown, R. S. Craxton, et al., Phys. Plasmas **3**, 2108 (1996).
[33] H. M. Antia, Astrophys. J. Suppl. Ser. **84**, 101 (1993).
[34] R. Zimmermann, *Many-Particle Theory of Highly Excited Semiconductors* (Teubner Verlag, Leipzig, 1988).